Scattering Study on the Selective Solvent Swelling Induced Surface Reconstruction

Ting Xu,[†] James T. Goldbach,[†] Matthew J. Misner,[†] Seunghyun Kim,[†] Alain Gibaud,[‡] Oleg Gang,[§] Ben Ocko,[§] Kathryn W. Guarini,[⊥] Charles T. Black,[⊥] Craig J. Hawker,[#] and Thomas P. Russell*[,†]

Department of Polymer Science and Engineering, University of Massachusetts, Amherst, Massachusetts 01003; Faculté des Sciences, Université du Maine, Avenue O. Messiaen, 72085 Le Mans Cedex 09, France; Department of Physics, Brookhaven National Laboratory, Upton, New York 11973; IBM T. J. Watson Research Center, Yorktown Heights, New York 10598; and IBM Almaden Research Center, San Jose, California 95120

Received October 8, 2003; Revised Manuscript Received December 17, 2003

ABSTRACT: A selective solvent induced surface reconstruction of thin films of an asymmetric diblock copolymer of poly(styrene-*b*-methyl methacrylate) was investigated by grazing incidence small-angle X-ray scattering, X-ray reflectivity, and atomic force microscopy. It is quantitatively shown that the selective swelling of the minor component results in the formation of a nanoporous film where the initial hexagonal array of the copolymer is preserved without affecting the lattice constant, 40.7 nm. However, the film thickness increased by ∼17%, and the average electron density decreased by ∼20%. The electron density profiles obtained by fitting the X-ray reflectivity indicate that the pores penetrate through the entire film and that the pores are oriented normal to the surface.

Introduction

Block copolymers offer simple routes for the rapid fabrication of arrays of nanoscale structures over large surface areas.[1−8] By balancing the interfacial interactions, the copolymer microdomains can be oriented normal to the surface.[2,5,6,9−13] Previous studies have shown that poly(styrene-*b*-methyl methacrylate) (P(S-*b*-MMA)) thin films can be prepared with the cylindrical microdomains oriented normal to the surface. Selectively removing the minor (PMMA) component along with cross-linking the PS matrix by deep UV exposure and solvent rinsing produces a nanoporous film.[14] Recently, selective solvent swelling was reported as a simpler alternate route to the same end.[15,16] Here the PMMA block was drawn to the surface by immersing the films in acetic acid, a selective solvent for PMMA. Upon drying, the PMMA was trapped at the surface, thereby generating the nanoporous films. This process is fully reversible, where, upon heating the film above the glass transition temperature, the original array of cylindrical domains oriented normal to the surface is recovered. These initial observations were based on electron microscopy and atomic force microscopy experiments, and a quantitative measure of the depth and shapes of the pores was not possible.

High-resolution X-ray scattering measurements, however, provides sufficient spatial resolution, and sensitivity to the internal structure, so that a detailed description of the surface reconstruction process can be obtained. Specifically, grazing incidence small-angle X-ray scattering (GISAXS) provides information on the lateral and internal ordering of the copolymer film before and after the solvent induced reconstruction. X-ray reflectivity, on the other hand, provides a measure of the average file properties, including the total thickness and the average electron density. The combined results indicate that the pores span the entire film thickness and that the lateral spacing of the pore was not affected by the solvent swelling.

Experimental Section

Asymmetric diblock copolymers of polystyrene and poly(methyl methacrylate) (P(S-*b*-MMA)) with an average molecular weight of 69 000 and polydispersity of 1.04 with a PMMA volume fraction of 0.29 were synthesized anionically. Silicon substrates with balanced interfacial interactions to polystyrene (PS) and poly(methyl methacrylate) (PMMA) were prepared by anchoring a random copolymer of styrene and methyl methacrylate (58% PS) to the native silicon oxide layer as described before.[9,17] A film of poly(styrene-*block*-methyl methacrylate) (P(S-*b*-MMA)) with a thickness near the repeat period was spin-coated onto the substrates and annealed at 170 °C under vacuum for 40 h. Half of the film was subjected to the acetic acid (20 min) and deionized water rinses (20 min). Tapping mode AFM was performed with a Dimension 3100, Nanoscope III from Digital Instruments Corp. Grazing incident small-angle X-ray scattering (GISAXS) was performed on the beamline X22B at NSLS, Brookhaven National Laboratory, using X-rays with a wavelength of 1.567 Å. The exposure time was 20 s per frame. The transverse and longitudinal coherence lengths are ∼1−2 μm. X-ray reflectivity was performed using X-rays with a wavelength of 1.15 Å at beamline X22A at NSLS. Using the dynamical theory, the matrix method was used to analyze the reflectivity data.

Results and Discussion

For thin films with small numbers of scattering centers in the scattering volume, grazing incident small-angle X-ray scattering (GISAXS), especially with the use of high-intensity synchrotron radiation source, is a powerful technique to study the lateral ordering.[18−24] GISAXS has several advantages over conventional transmission scattering, including (i) the absorption of X-rays by the substrate is irrelevant, (ii) the surface

[†] University of Massachusetts.
[‡] Université du Maine.
[§] Brookhaven National Laboratory.
[⊥] IBM T. J. Watson Research Center.
[#] IBM Almaden Research Center.

10.1021/ma0355204 CCC: $27.50
Published on Web 03/20/2004

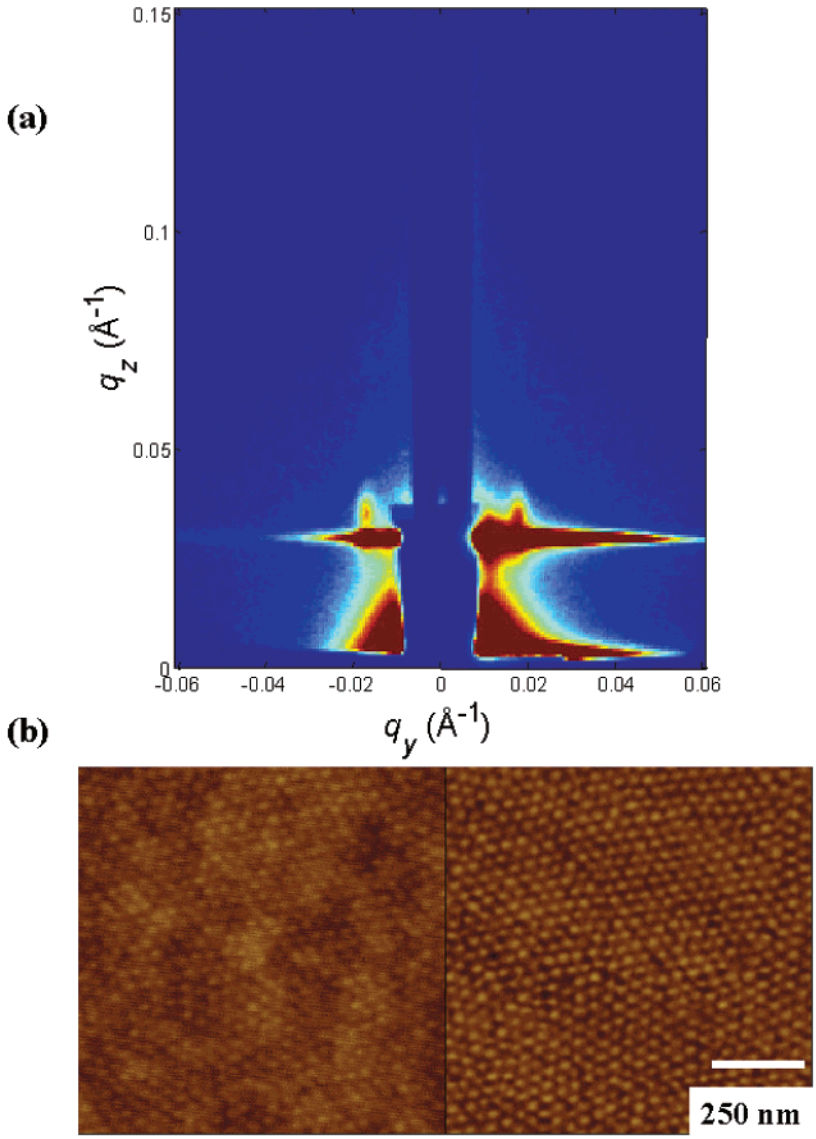

Figure 1. (a) Grazing incidence small-angle X-ray scattering patterns of the P(S-*b*-MMA) film on a silicon substrate modified with random copolymer after annealing at 170 °C under vacuum for 40 h and (b) atomic force microscopy height (left) and phase (right) images ($1 \times 1\ \mu m^2$) of the film.

scattering geometry enables studies on ultrathin films, and (iii) the large area of illumination provides information averaging over the length of the sample. The X-ray beam impinges at a grazing angle onto the sample slightly above the critical angle, so that the film is still fully penetrated by the X-rays. The intensity in the scattering plane is determined by the specular and off-specular reflectivity that contains information on the laterally averaged density profile normal to the substrate. Defining the incident angle as α_i, the exit angle as α_f (parallel to the surface), and out-of-plane angles as ψ (normal to the surface), with the sample surface as the (x, y) plane and the incidence beam along the x-axis, a scattering vector $\bar{q}(q_x,q_y,q_z)$ is calculated using $q_x = (2\pi/\lambda)(\cos(\psi)\cos(\alpha_f) - \cos(\alpha_i))$, $q_y = (2\pi/\lambda)\sin(\psi)\cos(\alpha_f)$, and $q_z = (2\pi/\lambda)(\sin(\alpha_f) + \sin(\alpha_i))$. Since the incident angle α_i is very small, the GISAXS signal mainly depends on the in-plane vector component q_y that is related to the lateral ordering in the sample and the out-of-plane vector component q_z that is related to the ordering in the depth direction.

In Figure 1a we show the GISAXS pattern for the initially prepared (prior to swelling) P(S-*b*-MMA) film at a grazing incidence angle $\alpha \approx 0.2°$. The pattern shows two features at $q_y = 0.178\ nm^{-1}$, which are diffuse along q_z. These peaks come from the hexagonal lateral packing of the cylindrical microdomains with an orientation normal to the surface. In Figure 1b, the corresponding AFM height and phase images of the film are shown. These images show hexagonally packed PMMA cylindrical microdomains oriented normal to the surface with surface roughness ~0.4 nm. The GISAXS pattern and height and phase AFM images of a film after dipping in acetic acid and rinsing with deionized water are shown in Figure 2. The AFM images show a hexagonally packed array of nanopores in the film with surface roughness ~1.2 nm. The GISAXS pattern after acetic acid rinsing is dramatically different from that of the initial film. A comparison of Figure 2a and Figure 1a shows a pronounced enhancement of the intensity and higher order features after rinsing.

Intensity profiles of the GISAXS patterns along q_y and q_z, i.e., parallel and perpendicular to the surface of the film, from the data in Figure 1a and Figure 2a, are shown in Figure 3. Scans along q_y (Figure 3a) show peaks characteristic of the in-plane periodicity of the

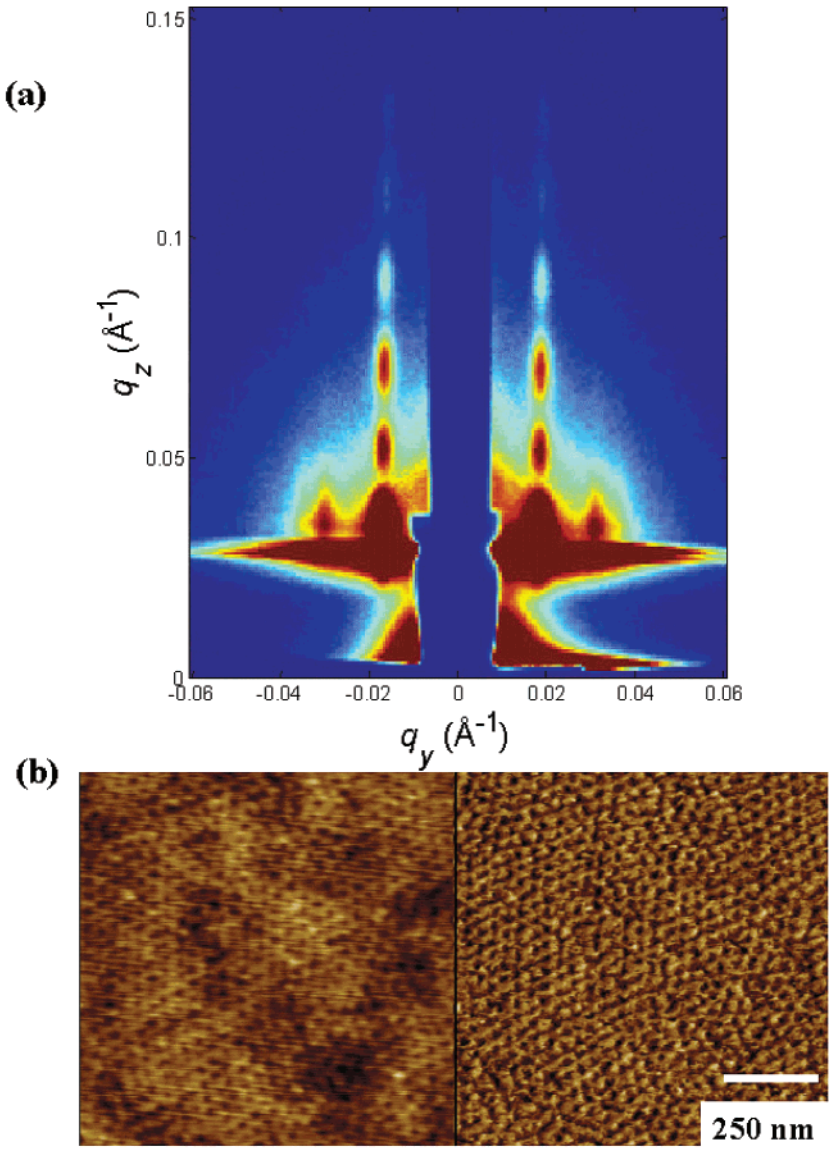

Figure 2. (a) Grazing incidence small-angle X-ray scattering patterns of the P(S-*b*-MMA) film on a silicon substrate modified with random copolymer after annealing at 170 °C under vacuum for 40 h and then rinsed in acetic acid and (b) atomic force microscopy height (left) and phase (right) images (1×1 μm^2) of the film after dipping with acetic acid.

films. Prior to swelling, only the first order is seen at 0.178 nm^{-1}. After swelling, three peaks, located at 0.178, 0.306, and 0.36 nm^{-1}, are observed. The positions of the peaks are consistent with a hexagonally packed array of cylinders normal to the surface with a center-to-center distance of 40.7 nm. It should also be noted that the positions of first-order reflection for the initial film and the nanoporous film are the same. Consequently, the lateral packing of the cylinders is invariant.

The absolute scatting cross section per unit volume, $d\Sigma/d\Omega$, for a two-phase system is given by the product of a contrast factor K and an interference function $S(q)$, where $S(q)$ is dictated by the shape and spatial arrangement of the phases. The contrast factor K is proportional to $\Delta\rho_e^2$, which is the square of the electron density difference between the two phases. In Figure 1a, one weak reflection along q_y is evident with no higher order reflections observable. The relatively low scattering intensity arises from the small $\Delta\rho_e^2$ between the PMMA and PS domains. With the formation of pores, a marked change in the X-ray contrast occurs. The relative contrast increase can be approximated as $(\rho_{ps}/(\rho_{pmma} - \rho_{ps}))$, which corresponds to a dramatic increasing in the intensity. This is consistent with the data in Figure 3.

The q_z scan shown in Figure 3b is measured along the first diffuse rod ($q_y = 0.178$ nm^{-1}) and shows oscillations with a period close to 0.185 nm^{-1}, corresponding to a thickness of ~34 nm. (This thickness is related to the fringes appearing in the modulus square of the Fourier transform of the electron density of the pores along the z direction.) The q_z scan provides a measurement of density distribution along the z direction. The observation of fringes out to 1.5 nm^{-1} suggests that the termination of the pores is sharp, on the nanometer length scale. Within the context of a model of uniform pore shape, independent of depth, the 33.8 nm thickness corresponds to the depths of the pores.

Since the electron density of air is zero, the electron density profile normal to the surface, as measured by X-ray reflectivity, corresponds to the shape of the pores and can be used to determine whether the pores penetrate through the entire film. In Figure 4 we show two potential models of the pores: in (a), the pores extend through the entire thickness of the film, whereas in (b), the pores only extend partially through the film.

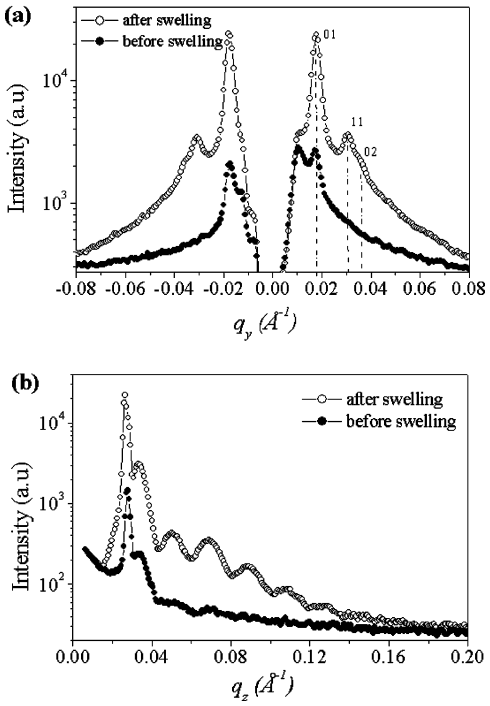

Figure 3. Scans of the GISAXS patterns in Figures 1a and 2a along (a) q_y direction at $q_z = 0.33$ nm^{-1} and (b) q_z direction at $q_y = 0.18$ nm^{-1}.

On the basis of the data presented below, we have ascertained that (a) describes the present data. In Figure 5, the measured reflectivity of the P(S-*b*-MMA) thin films (a) before swelling and (b) after swelling is shown as circles. Detailed information is obtained by fits of the calculated reflectivity using model electron density profiles. The solid lines are the best fits to the experimental data where the electron density profile obtained from the fits is shown in the inset. There is excellent agreement between the data and the fits over the entire scattering vector range.

The electron density profile of the film before swelling (inset of Figure 5a) indicates that the film consists of two layers: a random copolymer brush adjacent to the substrate and a uniform layer. The electron density difference between these two layers is quite small, and only the Kiessig fringes, characteristic of the total film thickness, are evident. After swelling and drying, the film is still composed of two layers. One is the ~7 nm random copolymer brush layer, and the second is the nanoporous film. Now, however, two frequencies are seen in the fringes of the reflectivity profile in Figure 5b. The high-frequency fringe corresponds to the total film thickness, and low-frequency one corresponds to the random copolymer brushes layer. The difference in the reflectivity profiles arises from the large decrease in the average electron density of the copolymer film due to the formation of pores and the generation of sufficient electron density contrast between the random copolymer brush and the porous film. The constant electron density of the porous film layer indicates that the pores fully penetrate the film. Thus, the schematic drawing in Figure 4a illustrates the generation of the nanoporous film by selective solvent swelling.

Since the electron density of the random copolymer brush layer is the same before and after swelling, this indicates that the acetic acid did not deteriorate the random brush. This is consistent with the reversibility of the swelling process. By heating the porous film, a film with an array of hexagonally packed PMMA cylinders oriented normal to the surface is regenerated. On the basis of the electron density profile, the thickness of the random copolymer brushes layer increases by ~1 nm, indicating a diffusion of the PMMA block

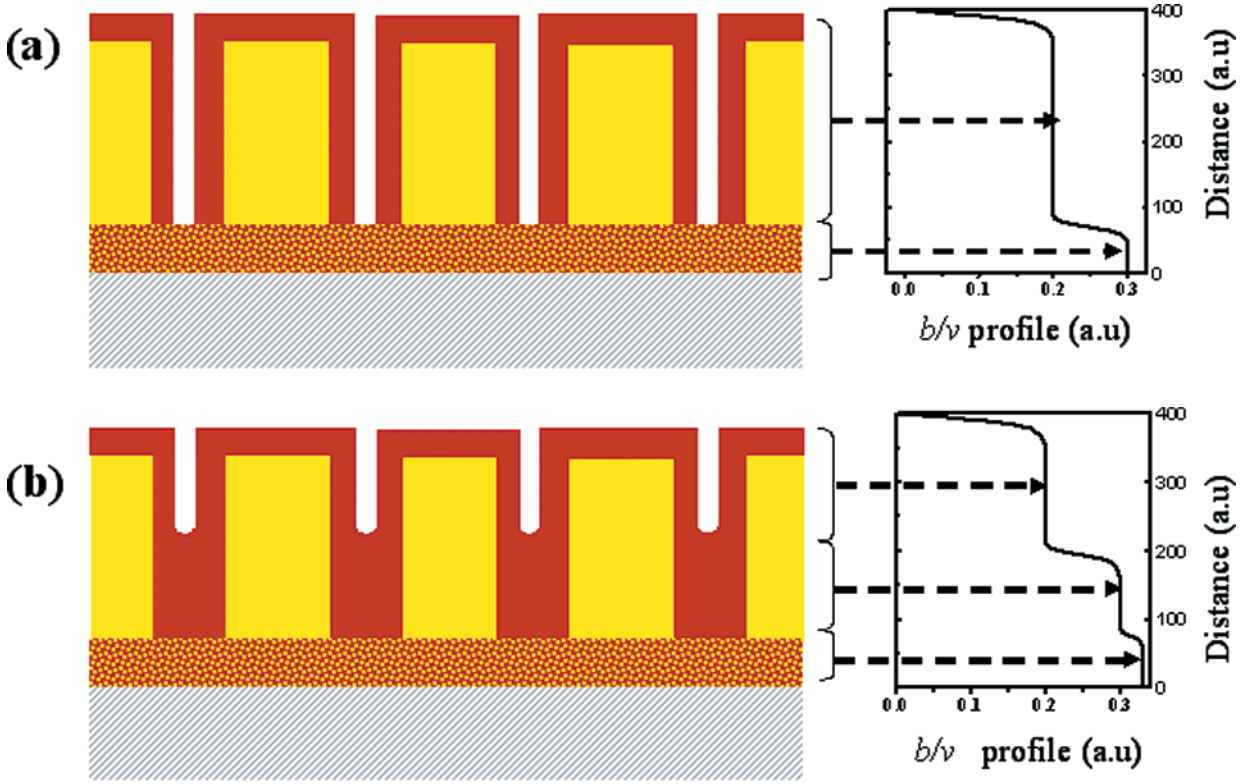

Figure 4. Schematic diagram of a porous block copolymer film with different pore penetration depth and corresponding electron density (b/V) profiles.

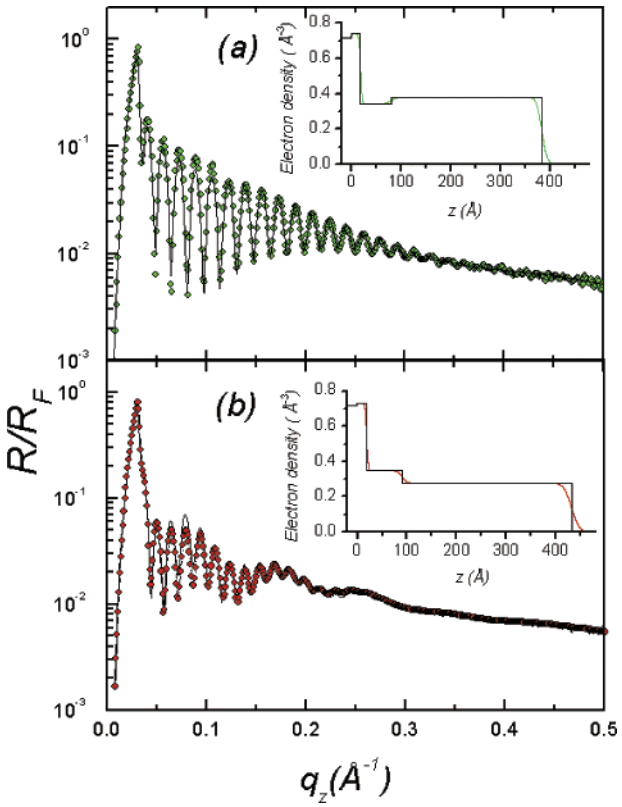

Figure 5. Measured X-ray reflectivity (circles) of the P(S-*b*-MMA) thin films (a) before swelling and (b) after swelling. The solid line in the figure is a fit to the experimental data, calculated using the electron density *b*/*V*, profile shown in the inset.

down into the brush layer. Since the random copolymer brush is soluble in acetic acid, the PMMA block of the copolymer can diffuse to substrate. This diffusion process is similar to the relocation of the PMMA block to the air/polymer interface and explains the origin of the formation of pores all the way through the film.

By comparing the reflectivity profiles before and after swelling, several changes are seen. First, the critical wave vector of the diblock copolymer film decreases from 0.22 to 0.196 nm^{-1} which translates into a decrease in the electron density from 344 to 273 e/nm^3. The formation of pores in the cylindrical microdomains accounts for the 20% reduction in the electron density. Second, the overall reflectivity decreases after swelling due the increase in the film roughness from 0.8 to 1.2 nm. Again, the formation of the pores increases the surface roughness as shown in the AFM height image in Figure 2b. Third, the frequency change of the fringes shows that after swelling the polymer film thickness increases from 30.4 to 34.8 nm, which can be explained by the reconstruction of the film, where the PMMA block is drawn to the surface, thereby increasing the film thickness, decreasing the electron density, and increasing the roughness. This value is in excellent agreement with the 33.8 nm thickness obtained from the q_z scan obtained from the GISAXS pattern. This conclusively shows that the depth of the holes is the same as the thickness of the diblock copolymer film.

Conclusion

In conclusion, grazing angle small-angle X-ray scattering and X-ray reflectivity were used to study a reconstruction in block copolymer films. A selective solvent induced reconstruction is shown where the minor component block is drawn to the surface of the film and upon drying generates a nanoporous film. GISAXS confirmed that the 40.7 nm lateral repeat period remained during the reconstruction. The electron density profiles derived from model calculation of the X-ray reflectivity profiles before and after swelling indicate the formation of pores that span the entire film while retaining the original lattice of the copolymer. Such a reconstruction represents a significant simplification of current methods to produce nanoporous films and demonstrates the power X-ray scattering methods offer for the quantitative characterization of such films.

Acknowledgment. This work was funded by the Department of Energy, Office of Basic Energy Sciences (DE-FG02-96ER45612), Material Research Science and Engineering Center (MRSEC) at University of Massachusetts, Amherst (DMR-0213695), and a National Science Foundation GOALI project (DMI-0217816). Work at Brookhaven National Laboratory is supported through the Department of Energy, Office of Basic Energy Sciences (DE-AC02-98CH10886), and from the Nanoscale Science, Engineering, and Technology Program.

References and Notes

(1) Park, M.; Harrison, C. K.; Chaikin, P. M.; Register, R. A.; Adamson, D. H. *Science* **1997**, *276*, 1401.
(2) Huang, E.; Rockford, L.; Russell, T. P.; Hawker, C. J.; Mays, J. *Nature (London)* **1998**, *395*, 757.
(3) Segalman, R. A.; Yokoyama, H.; Kramer, E. J. *Adv. Mater.* **2001**, *13*, 1152.
(4) Li, R. R.; Dapkus, P. D.; Thompson, M. E.; Jeong, W. G.; Harrison, C.; Chaikin, P. M.; Register, R. A.; Adamson, D. H. *Appl. Phys. Lett.* **2000**, *76*, 1689.
(5) Guarini, K. W.; Black, C. T.; Milkove, K. R.; Sandstrom, R. L. *J. Vac. Sci. Technol. B* **2001**, *19*, 2784.
(6) Black, C. T.; Guarini, K. W.; Milkove, K. R.; Baker, S. M.; Russell, T. P.; Tuominen, M. T. *Appl. Phys. Lett.* **2001**, *79*, 409.
(7) Cheng, J. Y.; Ross, C. A.; Chan, V. Z. H.; Thomas, E. L.; Lammertink, R. G. H.; Vancso, G. J. *Adv. Mater.* **2001**, *13*, 1174.
(8) Kim, S. H.; Misner, M. J.; Xu, T.; Kimura, M.; Russell, T. P. *Adv. Mater.*, in press.
(9) Mansky, P.; Liu, Y.; Huang, E.; Russell, T. P.; Hawker, C. J. *Science* **1997**, *275*, 1458.
(10) Kellogg, G. J.; Walton, D. G.; Mayes, A. M.; Lambooy, P.; Russell, T. P.; Gallagher, P. D.; Satija, S. K. *Phys. Rev. Lett.* **1996**, *76*, 2503.
(11) Lambooy, P.; Russell, T. P.; Kellogg, G. J.; Mayes, A. M.; Gallagher, P. D.; Satija, S. K. *Phys. Rev. Lett.* **1994**, *72*, 2899.
(12) Xu, T.; Kim, H. C.; DeRochy, J.; Seney, C.; Levesque, C.; Martin, P.; Stafford, C. M.; Russell, T. P. *Polymer* **2001**, *42*, 9091.
(13) Kim, H. C.; Jia, X. Q.; Stafford, C. M.; Kim, D. H.; McCarthy, T. J.; Tuominen, M.; Hawker, C. J.; Russell, T. P. *Adv. Mater.* **2001**, *13*, 795−797.
(14) Albrecht, T. T.; Steiner, R.; DeRouchey, J.; Stafford, C. M.; Huang, E.; Bal, M.; Tuominen, M.; Hawker, C. J.; Russell, T. P. *Adv. Mater.* **2000**, *12*, 787.
(15) Guarini, K. W.; Black, C. T.; Yeung, S. *Adv. Mater.* **2002**, *14*, 1290.
(16) Xu, T.; Stevens, J.; Villa, J.; Goldbach, J. T.; Guarini, K. W.; Black, C. T.; Hawker, C. J.; Russell, T. P. *Adv. Funct. Mater.* **2003**, *13*, 698.
(17) Benoit, D.; Chaplinski, V.; Braslau, R.; Hawker, C. J. *J. Am. Chem. Soc.* **1999**, *121*, 3904.
(18) Sinha, S. K.; Sirota, E. B.; Garoff, S.; Stanley, H. B. *Phys. Rev. B* **1988**, *38*, *2297*.

(19) Muller-Buschbaum, P.; Cubitt, R.; Petry, W. *Langmuir* **2003**, *19*, 7778.
(20) Factor, B. J.; Russell, T. P.; Tony, M. F. *Macromolecules* **1993**, *26*, 2847.
(21) Levine, J. R.; Cohen, L. B.; Chung, Y. W.; Georgopoulos, P. *J. Appl. Crystallogr.* **1989**, *22*, 528.
(22) Muller-Buschbaum, P. *Anal. Bioanal. Chem.* **2003**, *376*, 3.
(23) Doshi, D. A.; Gibaud, A.; Goletto, V.; Lu, M. C.; Gerung, H.; Ocko, B.; Han, S. M.; Brinker, C. J. *J. Am. Chem. Soc.* **2003**, *125*, 11646.
(24) Busch, P.; Smilgies, D.-M.; Posselt, D.; Kremer, F.; Papadakis, C. M. *Macromol. Chem. Phys.* **2003**, *204*, 18.

MA0355204